Journal of Alloys and Compounds 653 (2015) 168–174

Contents lists available at ScienceDirect

Journal of Alloys and Compounds

journal homepage: http://www.elsevier.com/locate/jalcom

Structural distortion, phonon behavior and electronic transition of Aurivillius layered ferroelectric $CaBi_2Nb_{2-x}W_xO_9$ ceramics

Kai Shi [a], Liang Peng [a], Mengjiao Li [a], Zhiyong Zhou [b], Kai Jiang [a], Jinzhong Zhang [a], Zhigao Hu [a, *], Xianlin Dong [b], Junhao Chu [a]

[a] Department of Electronic Engineering, East China Normal University, Shanghai 200241, China
[b] Key Laboratory of Inorganic Functional Materials and Devices, Shanghai Institute of Ceramics, Chinese Academy of Sciences, Shanghai 200050, China

ARTICLE INFO

Article history:
Received 18 July 2015
Received in revised form
19 August 2015
Accepted 6 September 2015
Available online 9 September 2015

Keywords:
Structural distortion
Phonon mode
Optoelectronic properties

ABSTRACT

The structure and optoelectronic properties of Aurivillius ferroelectric $CaBi_2Nb_{2-x}W_xO_9$ (CBNW, $x = 0$, 0.01, 0.03 and 0.05) ceramics have been studied. X-ray diffraction analysis shows that the ceramics exhibit the pure orthorhombic phase. The W dopant effects on phonon modes, Curie-temperature and optical band gap have been investigated by Raman scattering, temperature dependent dielectric permittivity and spectroscopic ellipsometry, respectively. The different behaviors of 595 cm^{-1}(ν_5) and 818 cm^{-1}(ν_6) phonon modes during the heating process are dominated by thermal expansion of the lattice and unusually positive anharmonic phonon coupling, respectively. Moreover, it was found that the distortion degree of (Nb, W)O_6 octahedra in ferroelectric phase of orthorhombic structure can be well discovered by the relative peak intensity of $I(\nu_6)/I[(\nu_5) + I(\nu_6)]$ ratio. Based on the value, it can be also inferred that the Curie temperature of $CaBi_2Nb_{2-x}W_xO_9$ decreases with increasing W composition, which is consistent with the results from temperature dependence dielectric permittivity. In addition, it is found that the optical band gap extends with increasing W composition by fitting the ellipsometric spectra with a three-layered model (air/surface roughness layer/ceramic). Meanwhile, the dielectric functions of CBNW ceramics have been uniquely extracted in the photon energy range of 1.8–5.5 eV. To explore the theoretical explanation on the experimental observations, the first-principles calculation on band structure and density of states were performed. It can be concluded that the hybridization between B-site atom orbital and O 2*p* (or Bi 6*p*) orbital is weakened by substituting W 5*d* for Nb 4*d*, which accounts for the variation of structure distortion and band gap.

1. Introduction

As an important branch of lead-free ferroelectric materials, bismuth layer-structured ferroelectrics (BLSFs) with Aurivillius phases were first described by Bengt Aurivillius [1]. Recently, they have gained increasing attention for the promising applications of non-volatile random access memories (NvRAMs), optical switches and high-temperature piezoelectric devices, because of their relatively high Curie-temperature (T_c), low dielectric dissipation, excellent hysteresis behavior, and fast switching voltage behavior [2,3]. The general chemical formula of Aurivillius phase materials is $[Bi_2O_2]^{2-}[A_{m-1}B_mO_{3m+1}]^{2+}$, where A is a mono-, di-, or triva-element with large 12 co-ordinate cation (e.g., Na^+, K^+, Ca^{2+}, Sr^{2+}, Ba^{2+}, La^{3+}, Y^{3+}, Pb^{3+}, Bi^{3+}…), B is a transition element with 6 co-ordinate cation(e.g., Fe^{3+}, Ti^{4+}, Nb^{5+}, Ta^{5+}, W^{6+}, Mo^{6+}…), and *m* (vary from 1 to 6) is the number of octahedral layers in perovskite slab $[A_mB_mO_{3m+1}]^{2+}$ between the adjacent $[Bi_2O_2]^{2-}$ [4,5]. For the materials with $m = 2$ in BLSFs with noncentrosymmetric space group $A2_1am$, the spontaneous ferroelectricity polarization along the *a* axis origins from the orthorhombic structure distortion, mainly containing the distortion of Bi_2O_2 layer and perovskite-type unit (BO_6 octahedra). It is feasible to improve the properties through A-site or B-site doping. For example, T_c changes from 300 °C to 440 °C in $SrBi_2(Ta_{1-x}Nb_x)_2O_9$, while it varies from 440 °C to about 940 °C in $Sr_{1-x}Ca_xBi_2Nb_2O_9$ as doping concentration increasing. Note that the variable range of T_c caused by B-site doping is narrower than that by A-site doping [6].

Calcium bismuth niobate ($CaBi_2NbO_9$, CBN) is an Aurivillius layered material with $m = 2$. Because of the ultra-high Curie

* Corresponding author.
E-mail address: zghu@ee.ecnu.edu.cn (Z. Hu).

http://dx.doi.org/10.1016/j.jallcom.2015.09.037
0925-8388/

temperature (T_c = 943 °C) among BLSFs and the relative higher thermal depoling temperature in polycrystalline ferroelectric ceramics, CBN is one of the most promising lead-free candidates for high-temperature (up to 800 °C) piezoelectric application [7]. The material applied in high-temperature piezoelectric field also needs high resistivity to reduce charge leakage effectively. It is coincidence that CBN doped with moderate tungsten (W, B-site doping) would increase the resistivity dramatically with changing T_c slightly [8–10]. The different properties induced by doping in BLSFs are always related to the structure distortion. Raman scattering is a nondestructive characterization technique, and a powerful tool to study lattice dynamics or symmetry disturbance. The spectra of vibration modes in different frequencies could be sensitive to describe the structural distortion. In addition, spectroscopic ellipsometry (SE) is an effective method for determining the dielectric functions of materials over a wide spectral range [11,12]. The dielectric function is directly related to the band structures and electronic transition by its imaginary part. However, few reports on optical properties of CBNW ceramics have been presented. Thus, it is meaningful to reveal the dielectric functions of CBNW for the potential applications in optoelectronic device.

In this article, X-ray diffraction (XRD), Raman scattering, temperature dependent dielectric permittivity and spectroscopic ellipsometry measurements of W-doped CBN have been studied. The evolution of phonon modes associated to the structure distortion in CBNW are discussed in detail. It is found that the relative peak intensity of $I(\nu_6)/I[(\nu_5)+I(\nu_6)]$ ratio can accurately described the structure distortion in CBNW ceramics. Moreover, the dielectric functions of ceramics in the near-infrared ultraviolet (NIR–UV) photon energy region are extracted by reproducing the experimental spectra with reasonable optical dispersion models. The tungsten composition effects on the electronic structure and optical band gap (E_g) have been discussed in detail. Further, the first-principles calculation on band structure and density of states were performed, which provide a reasonable explanation on the variation of structural distortion and optical band gap with different W composition.

2. Experimental details

The CBNW (x = 0, 0.01, 0.03 and 0.05, hereafter denoted W0, W1, W3 and W5, respectively.) ceramics were prepared by a conventional solid-state reaction processing, using the appropriate amount of starting raw materials of bismuth trioxide (Bi_2O_3), niobium pentoxide (Nb_2O_5), calcium carbonate ($CaCO_3$) and tungsten trioxide (WO_3). The samples were pressed into disks with the diameter of 13 mm and the thickness of 1 mm, then sintered at 1150 °C for 1 h in air atmosphere. All samples were rigorously single-side polished and cleaned in pure ethanol with an ultrasonic bath and rinsed several times by deionized water for the spectral measurements. The crystalline structures of CBNW ceramics were investigated by X-ray diffraction (XRD) using Cu $K\alpha$ radiation (D/MAX-2550V, Rigaku Co.). The temperature dependent Raman scattering measurements were carried out by a Jobin-Yvon LabRAM HR800UV micro-Raman spectrometer and a THMSE 600 heating/cooling stage (Linkam Scientific Instruments). The He–Ne laser with the wavelength of 632.8 nm was taken as the exciting source and the heating rate was controlled at 10 K/min during the temperature range from 100 K to 800 K with a step of 30 K, where the set-point stability is better than 0.5 K. The air-cooled charge coupled device (CCD) (−70 °C) with a 1024 × 256 pixels front illuminated chip was utilized to collect the scattered signal dispersed on 1800 grooves/mm grating. Temperature dependence of dielectric properties were characterized by an LCR meter (HP4284A, Hewlett–Packard, Palo Alto, CA) at 1 MHz from 300 K to 1240 K. The ellipsometric experiments measurements were carried out by a vertical variable-angle nearinfrared–ultraviolet optical ellipsometry (V-VASE by J.A. Woollam Co., Inc.) in the range of 1.8–5.5 eV. The spectral resolution of optical ellipsometry is set to 5 nm and the incident angle were selected as 65°, 70° and 75°. Ellipsometric data were directly analyzed with the WVASE32 software package.

3. Results and discussion

3.1. Structural analysis

Fig. 1 shows the XRD patterns performed on the polished surface of CBNW ceramics at room temperature (RT). The diffraction peaks are matched and indexed based on CBN crystal-structure parameters in Powder Diffraction File (PDF) No. 49-0608. It indicates that all CBNW samples are orthorhombic phase with the space group $A2_1am$ at RT. In addition, the partial substitution of Nb with W can keep pure single phase without other impurity phase structures since there are no peaks. The highest diffraction peak (115) for CBNW is consistent with the most highest diffraction peak in BLSFs, which exhibits Aurivillius phases should be (11 $2m+1$). The lattice constants were listed in Table 1. The value of a decreases from 5.496 Å to 5.484 Å as the W composition increases from 0 to 0.05. The compression of a with increasing W composition is resulted from the fact that the ionic radius of W^{6+} (0.60 Å) is smaller than that of Nb^{5+} (0.64 Å). The similar phenomenon can be also found in W-doped $SrBi_2Ta_2O_9$ [13]. The ratio of b/a, which is an indicator of the orthorhombic distortion, was shown in the inset of Fig. 1. It is known that ferroelectric phase of orthorhombic symmetry ($a \neq b$) is distorted from the paraelectric phase of tetragonal symmetry ($a = b$) in CBN [14]. Thus, the fact that the value of b/a rising close to 1 indicated that the orthorhombic distortion in CBNW is weakened. Note that the change of the lattice parameters could be the evidence of variation in structure distortion. Therefore, different Raman spectral response can be expected in CBNW ceramics with increasing W composition.

3.2. Raman scattering

As an example, Fig. 2(a) shows temperature-dependent Raman spectra of $CaBi_2Nb_{1.97}W_{0.03}O_9$ (W3) ceramic. Fig. 2(b) displays the

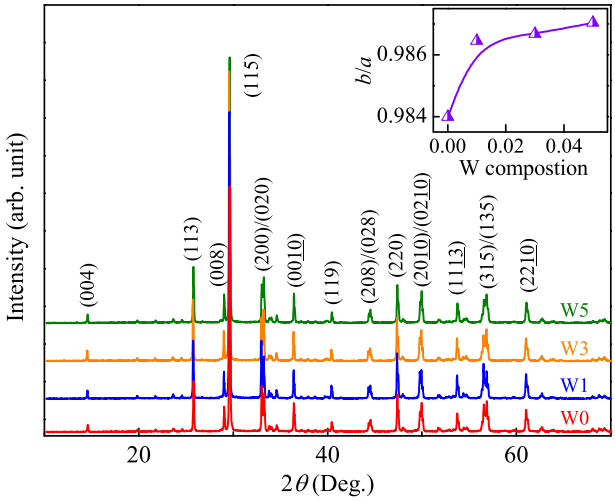

Fig. 1. X-ray diffraction patterns of the CBNW ceramics at room temperature with different W compositions. Some strong diffraction peaks are labeled. The inset shows the ratio of b/a with increasing W composition.

Table 1
The lattice constants and the best-fitting values of parameters in Eq. (1) for CBNW ceramics with different W compositions.

Samples	Lattice constants			Parameters				
	a (Å)	b (Å)	c (Å)	$\upsilon_{5,0}$ (cm^{-1})	$P_{5,1}$ (K^{-1})	$P_{5,2}$ (K^{-2})	A (cm^{-1})	B (cm^{-1})
W0	5.496	5.408	24.586	596.4	2.68×10^{-5}	4.62×10^{-8}	0.044	−0.0059
W1	5.491	5.416	24.652	596.4	3.49×10^{-5}	3.77×10^{-8}	0.033	−0.0087
W3	5.487	5.415	24.681	596.6	2.59×10^{-5}	5.83×10^{-8}	0.043	−0.0113
W5	5.484	5.413	24.617	596.5	3.33×10^{-5}	2.96×10^{-8}	0.060	−0.0199

spectra of the CBNW ceramics with different W compositions at 100 K. Note that, the temperature-dependent Raman spectra of other samples are similar. Group-theoretical analysis predicts 81 zone-center optical modes for CBN with $A2_1am$ (C_{2v}^{12}) orthorhombic symmetry. It is difficult to identify each phonon due to the mode overlapping with adjacent modes and the weaker intensity. Several main phonon modes are labeled in Fig. 2(b). The mode located at 66 cm^{-1} (ν_1) is recognized as the vibration of Bi^{3+} in the Bi_2O_2 layers, and the modes near at 185 cm^{-1} (ν_3) is associated with the vibration of Ca^{2+} ions in the perovskite-like layers. Moreover, the modes at about 164 cm^{-1} (ν_2) and 214 cm^{-1} (ν_4) correspond to the vibrations of Nb atoms in the x-y plane and z-axis, respectively. The modes located at around 595 (ν_5) and 819 cm^{-1} (ν_6) are assigned to the asymmetric and symmetric (Nb, W)–O vibration, respectively [6,15,16]. The similar spectra in Fig. 2(b) with different W compositions also confirm that CBN doped with tungsten can keep single phase. Fig. 2(a) suggests that the peak center of ν_5 deviated from the vertical dash line, and the color (in the web version) which represented the intensity of phonon mode faded with increasing temperature. This phenomenon means that the ν_5 phonon mode was soften. However, there is no obvious change in the ν_6 phonon mode upon heating, as compared to the behaviors of ν_5.

To further investigate the evolution of the ν_5 and ν_6 phonon modes, Raman spectra are well-fitted with multi-Lorentz oscillators. Fig. 3 shows Raman scattering results and well-fitted peaks with multi-Lorentz oscillators for all samples at 100 K, 300 K and 800 K. It can be seen that a good agreement is obtained between experimental and fitting spectra in the entirely measured range at different temperatures for all four ceramics. The frequency, intensity and full width at half maximum of each phonon mode at different temperature can be derived from the fitting. The frequencies of the ν_5 and ν_6 phonon modes for W3 are presented in Fig. 4(a). A continuous decrease of frequency can be seen in the ν_5 phonon modes, while that of ν_6 shows a slightly increase with increasing temperature. The similar trend could be also found in other samples. The shift of phonon modes can be explained by a simplified Klemens model [17]. In this model, the temperature

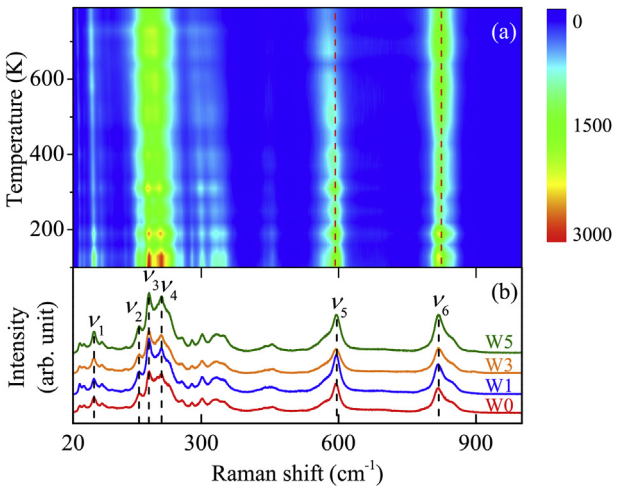

Fig. 2. (a) Temperature-dependence of Raman spectra of $CaBi_2Nb_{1.97}W_{0.03}O_9$ (W3) ceramics from 100 to 800 K. (b) Raman scattering of CBNW ceramics with different W compositions at T = 100 K.

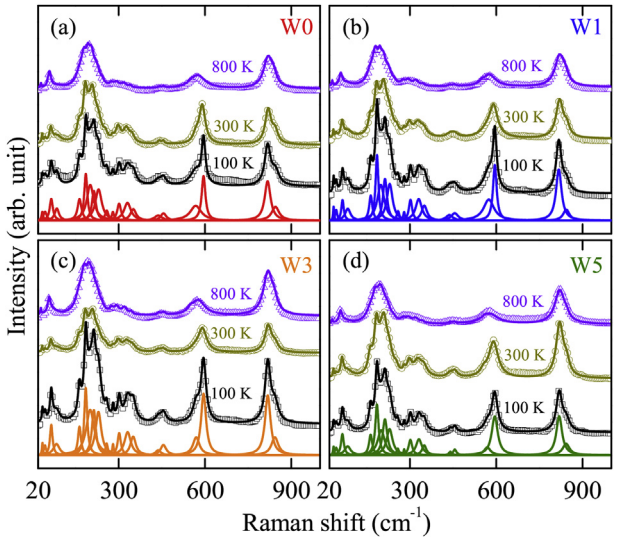

Fig. 3. Experimental (dots) and the best fitting (solid lines) Raman spectra of $CaBi_2Nb_{2-x}W_xO_9$ ceramics with (a) x = 0, (b) x = 0.01, (c) x = 0.03, and (d) x = 0.05 at 100 K, 300 K and 800 K, respectively.

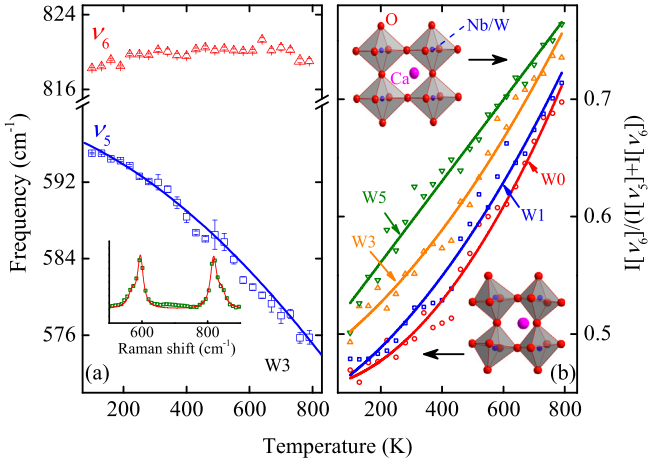

Fig. 4. (a) Temperature-dependence of phonon frequency of ν_5 (squares) and ν_6 (trilateral), the solid line represents the fitting of the experimental data using Eq. (1). Note that the inset is the fitting Raman spectra of W3 at 100 K with the range from 500 to 900 cm^{-1} (b) The relative intensity ratio of $I(\nu_6)/I[(\nu_5) + I(\nu_6)]$ with different W compositions. The ratios are linearly and/or nonlinearly fitted with the solid lines to guide the eyes. Schematic view of low distortion (up) and high distortion (down) (Nb, W)O_6 octahedra are insetted.

dependence of frequency (ν) is written as:

$$\nu_i(T) = \nu_{i,0} + \Delta\nu_{i,1}(T) + \Delta\nu_{i,2}(T). \quad (1)$$

where $\nu_{i,0}$ is the intrinsic harmonic frequency, $\Delta\nu_{i,1}(T)$ is the lattice expansion and thermal evolution contribution to the frequency, $\Delta\nu_{i,2}(T)$ is the contribution by intrinsic anharmonic coupling of phonons. The lattice contribution is usually expressed as the equation:

$$\Delta\nu_{i,1}(T) = \nu_{i,0}\left[\exp\left[-\int_0^T \gamma_i\alpha(T)dT\right] - 1\right]. \quad (2)$$

where $\gamma_i = -\partial ln\nu_i/\partial lnV$ is the Grüneisen parameter of mode i and $\alpha(T) = 1/V\partial V/\partial T$ is the coefficient of thermal expansion. Positive Grüneisen parameter can be obtained from the reports of Raman measurements under pressure for Aurivillius materials such as Bi_2MoO_6 ($m = 1$), $Bi_2W_2O_9$ ($m = 2$) and $Bi_4Ti_3O_{12}$ ($m = 3$) for the frequency of phonon over 500 cm^{-1} [18–20]. Thus, we can assume that the Grüneisen parameter will also be positive for ν_5 and ν_6 in CBNW. As for the coefficient of thermal expansion, the details of lattice expansion of Bi_3TiNbO_9 ($m = 2$) depend on temperature are investigated [21]. CBN possesses the similar properties and structure with Bi_3TiNbO_9. Therefore, it is reasonable to assume the thermal expansion coefficient α is positive and linear in CBNW, which is similar to that of Bi_3TiNbO_9. According to the above assumption, the exponential in $\Delta\nu_{i,1}(T)$ is <1, therefore, the contribution of $\Delta\nu_{i,1}(T)$ due to lattice expansion in ν_5 and ν_6 phonon modes is negative. The term related to anharmonic optical phonon coupling is given by:

$$\Delta\nu_{i,2}(T) = A\left[1 + \frac{2}{e^x - 1}\right] + B\left[1 + \frac{3}{e^y - 1} + \frac{3}{(e^y - 1)^2}\right]. \quad (3)$$

where $x = hc\nu_{i,0}/2k_BT$, $y = hc\nu_{i,0}/3k_BT$. h, c and k_B denote Planck's constant, the speed of light and Boltzmann's constant, respectively. The magnitude and signs of A and B represent the third- and forth-order contribution of anharmonic coupling phonons, which can be positive or negative.

To estimate different contribution of $\Delta\nu_1$ and $\Delta\nu_2$ to frequency shift, Eqs. (2) and (3) are substituted in Eq. (1) to give us the fitting expression, in which $\gamma_i\alpha(T)$ is linear to temperature is set to a fitting parameter with the form of $P_{i,1} + P_{i,2}T$. The well fitting result of parameters with different W compositions are also listed in Table 1. The magnitudes of $P_{i,1}$ and $P_{i,2}$ are in the same with $\alpha(T)$ of Bi_3TiNbO_9, which proves the rationality of the fitting result. From the fitting result, it is found that $\Delta\nu_{5,2}$ is approximately equal to 0. Thus, we can conclude that the frequency shift of ν_5 is dominated by the lattice expansion and thermal evolution. The influence of intrinsic anharmonic coupling of phonons to ν_5 is quite weak. In the case of ν_6, it is difficult to obtain reasonable parameters using Eq. (3). The observed slightly blue shift of ν_6 is quite different from the behaviors of ν_5, which may be ascribed to the unusually strong and positive intrinsic anharmonicity instead of thermal evolution.

From Fig. 2(b), it can be found that the intensity of ν_6 is lower than that of ν_5 in W0 and W1, while they are almost equivalent in W3 and W5. It means that the relative intensity of ν_6 to ν_5 is strengthened with increasing the W composition. The temperature evolutions of the relative peak intensity of $I(\nu_6)/I[(\nu_5) + I(\nu_6)]$ ratio with different W composition are plotted in Fig. 4(b). It can be clearly seen that the ratio of all samples increase with increasing W composition and temperature. For the distortion of (Nb, W)O_6 octahedra decreasing during heating [22], and the BO_6 octahedra distortion predominates the structure distortion in niobate with Aurivillius phase [23]. Thus, it can be inferred that the structure distortion in CBNW decreases with increasing W composition, which is consistent with the result of XRD. The parameter T_c generally decreases with the decrease of structure distortion degree [24,25]. Thus, the T_c in CBNW will drops as increasing W composition. To verify the inference derived from the relative intensity of $I(\nu_6)/I[(\nu_5) + I(\nu_6)]$ ratio, temperature dependence of dielectric permittivity was measured.

3.3. Dielectric characteristics

Fig. 5 illustrates temperature dependence of dielectric permittivity for CBNW with different composition at 1 MHz. It is well-known that the dielectric parameter measured by temperature dependence of dielectric permittivity is the real part of the complex dielectric function $\tilde{\varepsilon}(\omega) = \varepsilon_1 + i\varepsilon_2$, and an anomaly could be usually observed in the dielectric spectrum for ferroelectric, which corresponds to transition from ferroelectric to paraelectric [26]. The temperature, where the ε_1 reaches its maximum, is designated as Curie-temperature (T_c). In Fig. 5, it is found that the dielectric anomaly can be observed in all CBNW ceramics, and the T_c of CBNW with different W composition is presented in the inset of Fig. 5. It can be seen that pure CBN has a T_c value of 1213 K (940 °C), which is in good agreement with that reported by Yan et al. [7]. Meanwhile, T_c of CBNW ceramics gradually decreased from 1213 to 1206 K with the increasing of W composition, which is consistent with result inferred from the relative peak intensity of $I(\nu_6)/I[(\nu_5) + I(\nu_6)]$ ratio.

3.4. Spectroscopic ellipsometry

For the design of optoelectronic device, it is essential to obtain the optical response behaviors in visible–ultraviolet photon energy range, which are related to the complete complex dielectric function $\tilde{\varepsilon}(\omega)$. On the other hand, the imaginary part of $\tilde{\varepsilon}(\omega)$ is directly related to the band structures. Thus, spectroscopic ellipsometry experiments were performed to derive the complex dielectric function $\tilde{\varepsilon}(\omega)$.

SE, based on the reflectance configuration, is a sensitive and nondestructive optical method that measures the relative changes in the amplitude and the phase of particular directions of polarized light upon oblique reflection from the sample surface. The

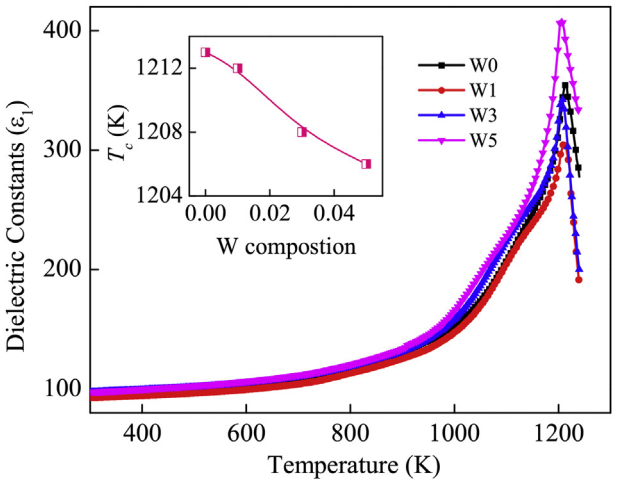

Fig. 5. Temperature-dependence of dielectric permittivity at 1 MHz of CBNW ceramics with different W compositions. The inset shows the value of T_c with increasing W composition.

experimental quantities measured by SE are the complex ratio $\tilde{\rho}(E)$ in terms of the angles $\Psi(E)$ and $\Delta(E)$, which are related to the structure and optical characterization of materials. In order to extract the dielectric functions $[\tilde{\varepsilon}(\omega) = \varepsilon_1 + i\varepsilon_2]$ and other significant physical parameters of CBNW ceramics, the ellipsometric spectra were evaluated by a three-layer model (air/surface roughness layer (SRL)/ceramic) [27]. Brüggeman effective-medium approximation (EMA) with a mixture of the bulk material (50%) and void (50%) was applied to model the surface roughness layer. It should be emphasized that the reliability of the fitting method mainly depends on the selection of the dielectric function models. Tauc-Lorentz (TL) model is one of the useful functions expressing the interband transition contributions, which has been applied in many semiconductor and dielectric materials successfully (e.g. ZnO, $BiFeO_3$, HfO_2…) [28–30]. Therefore, a single Tauc-Lorentz (TL) oscillator was applied to obtain optical properties of the CBNW ceramics. The ε_1 (the imaginary part) and ε_2 (the real part) of the complex dielectric function in TL model can be written as:

$$\varepsilon_2(E) = \begin{cases} \dfrac{A_0 E_n C (E - E_g)^2}{\left(E^2 - E_n^2\right)^2 + C^2 E^2} \dfrac{1}{E} & (E > E_g), \\ 0 & (E \le E_g). \end{cases} \tag{4}$$

$$\varepsilon_1(E) = \varepsilon_\infty + \frac{2}{\pi} P \int_{E_g}^{\infty} \frac{\xi \varepsilon_2(\xi)}{\xi^2 - E^2}. \tag{5}$$

where ε_∞ is the high-frequency dielectric constant, P is Cauchy principal part of the integral and E is the incident photon energy. Also, A_0, E_n, C and E_g are the amplitude, peak transition energy, broadening term, and Tauc gap energy of the oscillator, respectively. The ε_1 and ε_2 of the complex dielectric function in above TL model follows the Kramers–Krönig transformation (KKT).

For example, the experimental ellipsometric spectra Ψ and Δ of CBNW ceramics are shown by dotted lines in Fig. 6(a) and (b). The dielectric functions of the ceramics can be extracted by fitting TL dielectric functions model to the measured data. The fitted parameter values in Eqs. (4) and (5), and the thickness of SRL are summarized in Table 2. The simulated ellipsometric spectra for CBNW ceramics are also shown by the solid lines in Fig. 6(a) and (b). It can be seen that a good agreement is obtained between the experimental and calculated spectra in the entirely measured photon energy range and at different incident angles (65°, 70° and 75°). The evaluated dielectric function $[\tilde{\varepsilon}(\omega) = \varepsilon_1 + i\varepsilon_2]$ of the CBNW ceramics are shown in Fig. 6(c). ε_1 and ε_2 with the photon energy are the typical optical response behaviors of dielectric materials. As we can see from Fig. 6(c), the imaginary part ε_2 of $\tilde{\varepsilon}(\omega)$ is zero in the region E < E_g, and remarkably increases beyond E_g. It indicates a strong optical absorption appears, showing the interband electronic transition from the valence band (VB) to the lowest conductive band (CB). Meanwhile, the parameter ε_1 increases with the photon energy and approaches the maximum value around 4.5 eV, then decreases with further increasing photon energy because of the known Van Hove singularities.

The model parameters for optical band gap (E_g) are shown in Fig. 6(d). It is found that the value of E_g is about 3.4 eV for CBNW. This value fit well with similar Aurivillius layered materials such as $BaBi_2NbO_9$, Bi_3TiNbO_9 and $Bi_4Ti_3O_{12}$ which are all about 3.3 eV, and the similarity of the band gap is due to the similar BO_6 octahedra [31]. From Fig. 6(d), it is found that the value of E_g increases with the

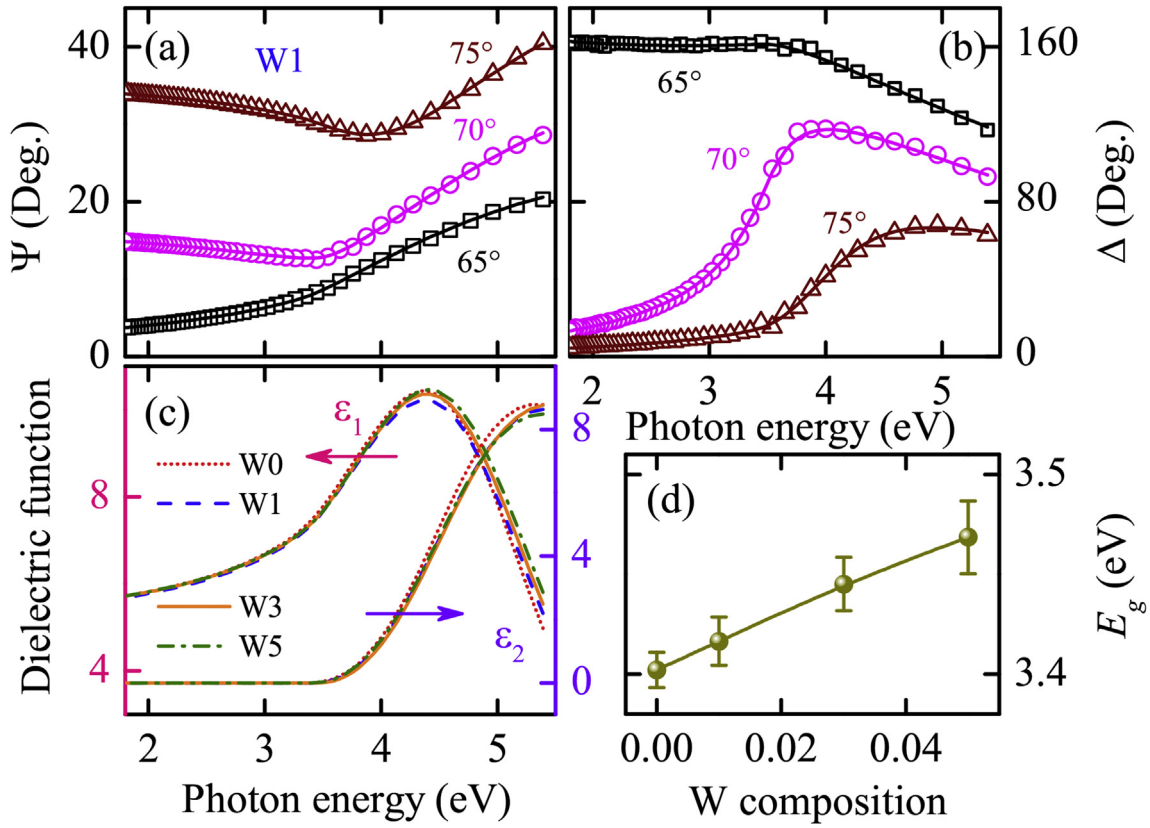

Fig. 6. Experimental (dots) and the best fitting (solid lines) ellipsometric spectra of (a) Ψ (E) and (b) Δ (E) recorded with various incident angle at 65°, 70° and 75° for W1. Evolution of (c) the real part ε_1 and the imaginary part ε_2 of the CBNW ceramics in the photon energy ranges from 1.8 to 5.5 eV. (d) The optical band gap E_g with increasing W composition.

Table 2
Dielectric function parameters of the Tauc-Lorentz model for CBNW ceramics with different W compositions determined form the simulation of ellipsometric spectra. Note that d_s is the thickness of the surface rough layers.

Samples	ε_∞	A_0 (eV)	E_g (eV)	E_n (eV)	C (eV)	d_s (nm)
W0	2.01 ± 0.02	207 ± 4	3.40 ± 0.01	4.86 ± 0.01	2.50 ± 0.02	5.8 ± 0.1
W1	1.97 ± 0.03	265 ± 5	3.42 ± 0.01	4.87 ± 0.01	2.65 ± 0.03	4.1 ± 0.1
W3	1.90 ± 0.03	223 ± 6	3.45 ± 0.01	4.88 ± 0.02	2.68 ± 0.03	4.0 ± 0.1
W5	1.79 ± 0.05	233 ± 9	3.47 ± 0.02	4.89 ± 0.02	2.75 ± 0.05	4.9 ± 0.1

W composition. In order to explain the phenomenon in experiments and obtain the electronic band structure, we performed first-principles calculation.

3.5. Electronic band structure

In the following work, the plane-wave-based density-functional theory (DFT) calculation with the generalized gradient approximation (GGA) was carried out for pure CBN in orthorhombic phase to obtain the information about the energy structure. The Perdew-Burke-Ernzerhof (PBE) functionals are used to address exchange–correlation interactions along with a standard plane-wave basis set with a kinetic-energy cutoff of 360 eV [32]. These calculations are performed by using the 12 × 12 × 3 Monkhorst-Pck k-point mesh, and the convergence criterion for the electronic energy is 10^{-6} eV. Fig. 7(a) and (b) show the band structure and density of states (DOS) of pure CBN in orthorhombic phase. The solid arrow located at the point of symmetry Y (0.5, 0.5, 0.5) in Fig. 7(a) indicates the direct electron transitions of optical band gap, which is approximately 2.44 eV. As a well-known problem of calculations based on DFT, the calculated optical band gaps are underestimated by about 20%–30%, as compare to the value derived from the TL model [33]. More importantly, the top valence bands (VBs) consist of O 2*p* states. On the other hand, the bottom of conduction bands (CBs) comes mainly from the hybridization of Bi 6*p*, Nb 4*d* and O 2*p* states.

It has been verified that the orbital hybridization and covalency play an crucial role in structural distortion and band structure of ferroelectric [34]. When Nb replaced by W partially, W 5*d* states will be introduced in CBs. However, the W 5*d* orbital is more extended than the Nb 4*d* orbital. Thus, the replacement of Nb with W cation will shift the bottom of conduction bands to the higher energy states, which will result in the enlargement of band gap in CBNW. The similar phenomenon could also found in $V_{1-x}W_xO_2$, $PbTi_{1-x}Zr_xO_3$ and $BaTi_{1-x}W_xO_3$, in which W 4*d*, Zr 4*d* orbital is more extended than the Ti 3*d* and V 3*d*(or Ti 3*d*) orbital, respectively [36,35,37]. Moreover, the replacement of Nb with W cation will weaken the hybridization strength between the Nb 4*d* (W 5*d*) and O 2*p* or Bi 6*p* orbitals and further its covalent bond energy of Nb–O (W–O) bond [38]. A NbO_6 octahedron is formed by the strongly hybridizes of Nb 4*d* orbital and O 2*p* orbital in CBN [22]. The NbO_6 distortion in ferroelectric orthorhombic phase is caused by the unequivalent Nb–O bonds. Since the weak hybridization of W 5*d* orbital and O 2*p* orbital will drops the bonding energy of B–O, the lower bonding energy could symmetrize six (Nb, W)–O bonds in the (Nb, W)O_6 octahedra, which can well explain the increases of *b*/*a* with W composition. Therefore, it can be also expected that W substituting for Nb would weaken the structural distortion and lower the Curie temperature T_c in CBNW.

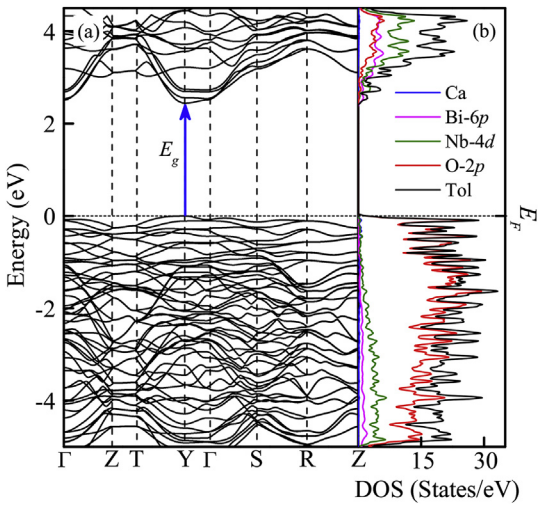

Fig. 7. Calculated (a) band structure and corresponding (b) density of states for pure CBN.

4. Conclusion

In summary, W doped calcium bismuth niobate with different composition (x = 0, 0.01, 0.03, 0.05) have been prepared by a conventional solid-state reaction process. The structural distortion, phonon behaviors and electronic structures have been investigated in detail. It is proved that ν_5 mode damping with temperature is dominated by the lattice expansion, while that of ν_6 mode is the unusually strong and positive intrinsic anharmonic phonon coupling. In addition, the structural distortion can be well indicated by relative intensity of $I(\nu_6)/I[(\nu_5) + I(\nu_6)]$ ratio. Moreover, the dielectric functions in the NIR–UV photon energy region have been uniquely extracted by fitting the measured ellipsometric data with a three-layered model. The optical band gap of CBNW is about 3.4 eV, and increases slightly with the W composition. The variation of structural distortion and optical band gap have been well explained in theory.

Acknowledgments

One of the authors (K. Shi) would like to thank Dr. Jiajun Zhu for constructive discussions. This work was financially supported by Major State Basic Research Development Program of China (Grant Nos. 2011CB922200 and 2013CB922300), Natural Science Foundation of China (Grant Nos. 11374097 and 61376129), Projects of Science and Technology Commission of Shanghai Municipality (Grant Nos. 15JC1401600, 14XD1401500, 13JC1402100 and 13JC1404200), and the Program for Professor of Special Appointment (Eastern Scholar) at Shanghai Institutions of Higher Learning.

References

[1] B. Aurivillius, Mixed bismuth oxides with layer lattices: I. The structure type of $CaNb_2Bi_2O_9$, Ark. Kemi 1 (1945) 463–480.
[2] C. A-Paz de Araujo, J.E. Cuchiaro, L.D. McMillan, M.C. Scott, J.F. Scott, Fatigue-free ferroelectric capacitors with platinum electrodes, Nature (London) 374 (1995) 627–629.
[3] D. Kajewski, Z. Ujma, Impedance analysis of thermally modified

$SrBi_2(Nb_{0.5}Ta_{0.5})_2O_9$ ceramics, J. Alloy. Compd. 509 (2001) 7532–7536.
[4] P.R. Graves, G. Hua, S. Myhra, J.G. Thompson, The Raman modes of the Aurivillius phases: temperature and polarization dependence, J. Solid State Chem. 114 (1995) 112–122.
[5] Yu. E. Kitaev, M.I. Aroyo, J.M. Perez-Mato, Site symmetry approach to phase transitions in perovskite-related ferroelectric compounds, Phys. Rev. B 75 (2007) 064110.
[6] S.M. Huang, Y.C. Li, C.D. Feng, M. Gu, X.L. Liu, Dielectric and structural properties of layer-structured $Sr_{1-x}Ca_xBi_2Nb_2O_9$, J. Am. Ceram. Soc. 91 (2008) 2933–2937.
[7] H.X. Yan, H.T. Zhang, R. Ubic, M.J. Reece, J. Liu, Z. Shen, Z. Zhang, A lead-free high-curie-point ferroelectric ceramic, $CaBi_2Nb_2O_9$, Adv. Mater. 17 (2005) 1261–1265.
[8] H.B. Chen, X.X. Guo, Z.H. Cui, J.W. Zhai, Donor and acceptor doping effects on the electrical conductivity of $CaBi_2Nb_2O_9$ ceramics, Phys. Status Solidi A 210 (2013) 1121–1127.
[9] Z.Y. Zhou, X.L. Dong, H. Chen, Structural and electrical properties of W^{6+}-Doped Bi_3 $TiNbO_9$ high-temperature piezoceramics, J. Am. Ceram. Soc. 89 (2006) 1756–1760.
[10] Z.Y. Zhou, Y.C. Li, S.P. Hui, X.L. Dong, Effect of tungsten doping in bismuth-layered $Na_{0.5}Bi_{2.5}Nb_2O_9$ high temperature piezoceramics, Appl. Phys. Lett. 104 (2014) 012904.
[11] S.G. Choi, R. Chen, C. Persson, T.J. Kim, S.Y. Hwang, Y.D. Kim, L.M. Mansfield, Dielectric function spectra at 40 K and critical-point energies for $CuIn_{0.7}Ga_{0.3}Se_2$, Appl. Phys. Lett. 101 (2012) 261903.
[12] S. Zhang, M.J. Han, J.Z. Zhang, Y.W. Li, Z.G. Hu, J.H. Chu, Optoelectronic and ferroelectric properties of cerium-doped $(Na_{0.5}Bi_{0.5})(Ti_{0.99}Fe_{0.01})O_3$ nanocrystalline films on (111) $Pt/TiO_2/SiO_2/Si$: a composition dependent study, ACS Appl. Mater. Interfaces 5 (2013) 3191–3198.
[13] I. Coondoo, N. Panwar, A.K. Jha, Effect of sintering temperature on the structural, dielectric and ferroelectric properties of tungsten substituted SBT ceramics, Phys. B 406 (2011) 374–381.
[14] M.P. Moret, R. Zallen, Infrared activity in the Aurivillius layered ferroelectric $SrBi_2Ta_2O_9$, Phys. Rev. B 57 (1998) 5715–5723.
[15] P.S. Dobal, R.S. Katiyar, Studies on ferroelectric perovskites and Bi-layered compounds using micro-Raman spectroscopy, J. Raman Spectrosc. 33 (2002) 405–423.
[16] M. Verma, K. Sreenivas, V. Gupta, Influence of La doping on structural and dielectric properties of $SrBi_2Nb_2O_9$ ceramics, J. Appl. Phys. 105 (2009) 024511.
[17] M. Balkanski, R.F. Wallis, E. Haro, Anharmonic effects in light scattering due to optical phonons in silicon, Phys. Rev. B 28 (1983) 1928–1934.
[18] G.A. Kourouklis, A. Jayaraman, L.G. Vanuitert, Pressure dependence of the Raman-active modes in $Bi_4Ti_3O_{12}$, Mater. Lett. 5 (1987) 116–119.
[19] M. Maczka, W. Paraguassu, P.T.C. Freire, A.G.S. Filho, J.M. Filho, J. Hanuza, Lattice dynamics and pressure-induced phase transitions in $Bi_2W_2O_9$: high-pressure Raman study, Phys. Rev. B 81 (2010) 104301.
[20] M. Maczka, P.T.C. Freire, C.L. Lima, W. Paraguassu, J. Hanuza, J.M. Filho, Pressure-induced phase transitions in ferroelectric Bi_2MoO_6-a Raman scattering study, J. Phys. Condens. Matter 22 (2010) 015901.
[21] A.V. Knyazev, O.V. Krasheninnikova, V.Z. Korokin, High-temperature characterization of some Aurivillius phases, Inorg. Mater. 50 (2014) 170–178.
[22] Y. Shimakawa, H. Imai, H. Kimura, S. Kimura, Y. Kubo, Orbital hybridization and covalency in paraelectric and ferroelectric $SrBi_2Nb_2O_9$, Phys. Rev. B 66 (2002) 144110.
[23] Y. Shimakawa, Y. Kubo, Structural distortion and ferroelectric properties of $SrBi_2(Ta_{1-x}Nb_x)_2O_9$, Appl. Phys. Lett. 77 (2000) 2749–2751.
[24] L. Sun, J.H. Chu, Analysis of relaxor mechanism and structural distortion for $SrBi_{1.6}Nd_{0.4}Nb_2O_9$ bismuth-layer-structured ceramics, Appl. Phys. Lett. 91 (2007) 242902.
[25] S.M. Blake, M.J. Falconer, M. McCreedy, P. Lightfoot, Cation disorder in ferroelectric Aurivillius phases of the type $Bi_2ANb_2O_9$ (A = Ba, Sr, Ca), J. Mater. Chem. 7 (1997) 1609–1613.
[26] E.V. Ramanaa, V.V. Kirana, T.B. Sankaram, Dielectric and pyroelectric properties of Sr-modified $(Na_{0.5}Bi_{0.5})$ $Bi_4Ti_4O_{15}$ ceramics, J. Alloy. Compd. 456 (2008) 271–276.
[27] J. Kvietkova, B. Daniel, M. Hetterich, M. Schubert, D. Spemann, D. Litvinov, D. Gerthsen, Near-band-gap dielectric function of $Zn_{1-x}Mn_xSe$ thin films determined by spectroscopic ellipsometry, Phys. Rev. B 70 (2004) 045316.
[28] H. Fujiwara, M. Kondo, Effects of carrier concentration on the dielectric function of ZnO:Ga and In_2O_3:Sn studied by spectroscopic ellipsometry: analysis of free-carrier and band-edge absorption, Phys. Rev. B 71 (2005) 075109.
[29] P. Chen, N.J. Podraza, X.S. Xu, A. Melville, E. Vlahos, V. Gopalan, R. Ramesh, D.G. Schlom, J.L. Musfeldt, Appl. Phys. Lett. 96 (2010) 131907.
[30] Y.J. Cho, N.V. Nguyen, C.A. Richter, J.R. Ehrstein, B.H. Lee, J.C. Lee, Spectroscopic ellipsometry characterization of high-k dielectric HfO_2 thin films and the high-temperature annealing effects on their optical properties, Appl. Phys. Lett. 80 (2002) 1249–1251.
[31] A. Peláiz-Barranco, Y. González-Abreu, Ferroelectric ceramic materials of the Aurivillius family, J. Adv. Dielectr. 3 (2013) 1330003.
[32] J.P. Perdew, K. Burke, M. Ernzerhof, Generalized gradient approximation made simple, Phys. Rev. Lett. 77 (1996) 3865–3868.
[33] J.Z. Zhang, W.Y. Tong, J.J. Zhu, J.Y. Xu, Z.H. Duan, L.P. Xu, Z.G. Hu, C.G. Duan, X.J. Meng, Z.Q. Zhu, J.H. Chu, Temperature dependent lattice dynamics and electronic transitions of $0.93Pb(Zn_{1/3}Nb_{2/3})O_3$-$0.07PbTiO_3$ single crystals: experiment and theory, Phys. Rev. B 91 (2015) 085201.
[34] R.E. Cohen, Origin of ferroelectricity in perovskite oxides, Nature (London) 358 (1992) 136–138.
[35] H.C. Chen, X. Lei, L.J. Yang, J.P. Long, Compositional effect of zirconium on structural, electronical, elastic and thermodynamic properties of $PbTi_{1-x}Zr_xO_3$, Superlatt. Microstruct. 64 (2013) 274–282.
[36] A.Y. Fasasi, R. Bucher, B.D. Ngom, U. Buttner, M. Maaza, C. Theron, E.G. Rohwer, Structural and optical properties of annealed W-doped $BaTiO_3$ thin films prepared by pulsed laser deposition, J. Phys. Condens. Matter 19 (2007) 466214.
[37] X.F. He, Y.J. Zeng, X.F. Xu, C.C. Gu, F. Chen, B.H. Wu, C.R. Wang, H.Z. Xing, X.S. Chen, J.H. Chu, Phys. Chem. Chem. Phys. 17 (2015) 11638–11645.
[38] Z.G. Hu, Y.W. Li, M. Zhu, Z.Q. Zhu, J.H. Chu, Composition dependence of dielectric function in ferroelectric $BaCo_xTi_{1-x}O_3$ films grown on quartz substrates by transmittance spectra, Appl. Phys. Lett. 92 (2007) 081904.